Heat- and pH-induced BSA conformational changes, hydrogel formation and application as 3D cell scaffold

Giovanna Navarra [a], Chiara Peres [a, 1], Marco Contardi [b, 1], Pasquale Picone [c], Pier Luigi San Biagio [b], Marta Di Carlo [c, ***, 2], Daniela Giacomazza [b, *, 2], Valeria Militello [a, **, 2]

[a] Dipartimento di Fisica e Chimica, Università di Palermo, Viale delle Scienze, Building 18, 90100, Palermo, Italy
[b] Istituto di Biofisica, Consiglio Nazionale delle Ricerche, Via U. La Malfa 153, 90100, Palermo, Italy
[c] Istituto di Biomedicina e Immunologia Molecolare, Consiglio Nazionale delle Ricerche, Via U. La Malfa 153, 90100, Palermo, Italy

ARTICLE INFO

ABSTRACT

Aggregation and gelation of globular proteins can be an advantage to generate new forms of nanoscale biomaterials based on the fibrillar architecture. Here, we report results obtained by exploiting the proteins' natural tendency to self-organize in 3D network, for the production of new material based on BSA for medical application. In particular, at five different pH values the conformational and structural changes of the BSA during all the steps of the thermal aggregation and gelation have been analyzed by FTIR spectroscopy. The macroscopic mechanical properties of these hydrogels have been obtained by rheological measurements. The microscopic structure of the gels have been studied by AFM and SEM images to have a picture of their different spatial arrangement. Finally, the use of the BSA hydrogels as scaffold has been tested in two different cell cultures.

© 2016 Elsevier Inc. All rights reserved.

1. Introduction

Many globular proteins have the ability to form gels, both by heat and cold treatments. It is well known that under appropriate conditions, native proteins can undergo conformational changes associated with partial unfolding or denaturation that may lead to aggregation [1,2] up to gelation, above a critical protein concentration [3]. Protein aggregation is a complex process made by different and simultaneous steps: first the protein partially unfolds and goes towards molten globule forms or intermediate states also called amorphous pre-aggregates [4,5]; second, these different aggregates in appropriate experimental conditions can form amorphous aggregates, fibrils and fibers [6]. Under appropriate conditions, depending on several factors among which the protein concentration, the temperature and the pH, these aggregates can be the bricks of protein hydrogels [7,8].

Recently, the fabrication of gels from biological molecules, in particular from proteins, has received increasing interest due to their applications in the field of biomedical research [9–12]. The protein-based hydrogels can be biocompatible and biodegradable [12], can entrap large amounts of water or biological fluids [13], have a microporous structure and provide an excellent mechanical support through their three-dimensional structure [14,15]. These properties make them ideal biomaterials also to be used as devices for encapsulation and protection of sensitive materials and pH-sensitive hydrogels for the controlled delivery of biologically-active drugs [16–18]. As an example, the microscopic and macroscopic properties of these hydrogels can be controlled by changing the pH value: particulate, brittle and opaque gel can be formed close to the protein isoelectric point, while more flexible and transparent gel, made of linear aggregates, far from the isoelectric point [19].

* Corresponding author.
** Corresponding author.
*** Corresponding author.
  E-mail addresses: giovanna.navarra@unipa.it (G. Navarra), chiara.peres85@gmail.com (C. Peres), marco.contardi@iit.it (M. Contardi), pasquale.picone@ibim.cnr.it (P. Picone), pierluigi.sanbiagio@cnr.it (P.L. San Biagio), di-carlo@ibim.cnr.it (M. Di Carlo), daniela.giacomazza@cnr.it (D. Giacomazza), valeria.militello@unipa.it (V. Militello).
  [1] Present address: Istituto Italiano di Tecnologia, Via Morego, 30, Genoa (Italy).
  [2] These authors share senior authorship.

Recent studies have demonstrated that gels formed by fibrillar aggregates are more prone to promoting cell attachment and neurite outgrowth, while hydrogels, having different structure, do not show any biological activity [15,20]. Thus, the well-known general tendency of the globular proteins to fibrillation and gelation can be taken as an advantage to generate new forms of nanoscale biomaterials based on the amyloid fibrillar architecture, since they are characterized by well-ordered and stable structures that can be formed by self-association in aqueous solution [21,22]. The surplus value, consisting in their highly ordered network stabilized by intermolecular and/or intramolecular hydrogen bonding, electrostatic interactions, and hydrophobic effects, makes the fibrillar hydrogels a versatile device usable as scaffold in tissue engineering [20]. Gels made by biocompatible physically cross-linked protein molecules, should be used for scaffolds, controlled drug delivery, or uptake of biological molecules [23]. Indeed, biodegradable hydrogels capable of phase transition in response to external stimuli such as temperature or pH values represent an alternative method of preparing injectable hydrogels for biomedical applications [23].

It is important to emphasize that the relevant properties of biocompatibility are not affected by using a gel formed by mature fibrils. Fibrils are the final state of aggregated and re-organized protofibrils and it is now established that prefibrillar oligomers [24–27] rather than mature fibrils are the prime toxic agents [27–29] responsible of the amyloid-induced cellular toxicity.

In this paper, we report results obtained by exploiting the natural tendency of bovine serum albumin (BSA) to self-organize in 3D network, for the production of new protein-based materials. The main aim of our work has been to determine the appropriate experimental conditions to obtain hydrogels of BSA aggregates and to characterized the hydrogels thus formed. Albumin is an abundant and low-cost protein with a molecular weight of 66 kDa, in some forms also human-compatible and with well-known properties [1,30,31]. It is an important natural carrier of hydrophobic molecules and a polyampholyte with pH-dependent charge. After heating or cooling treatments it can form hydrogels [32], ideal candidates for loading and releasing drugs, since its sites can be reversibly used to bind and release drugs by regulating pH value [18,33]. In this work we have characterized the conformation and the morphology of the BSA heat-induced aggregates, namely the fundamental "bricks" of the network, and investigated if the modifications of the pH and protein concentration can induce hydrogels with different structural properties when subjected to prolonged heating. The conformational and structural changes of the protein during incubation at 60 °C were studied by FTIR spectroscopy. The aggregation growth and the gelation process were followed by FTIR and rheological measurements up to 20 h from the beginning of the experiments. Information about the morphology of the aggregates during the gelation process were obtained by atomic force microscopy (AFM). Finally, micrographs of the different kinds of hydrogels were made by SEM measurements and biological tests on LAN5 cell cultures have been also performed. Our results indicate that it is possible to modulate the final texture of the hydrogels by tuning pH and protein concentration for the appropriate applications.

2. Experimental

2.1. Sample preparation

Bovine serum albumin was purchased from Sigma-Aldrich. Powdered protein was dissolved in the appropriate buffer solution, prepared in H_2O or D_2O (99.9%, Aldrich) to obtain the wanted pH (or pD). In particular, phosphate buffers 0.1 M was used to obtain pH 5.9, 7.4 and 8.5; samples prepared at pH 2.7 and 3.9 were made by diluting the protein powder in different amounts of KCl solution

0.1 M and HCl solution 1.2 M. The protein final investigated concentrations were 0.5 and 1 mM pH values have been corrected for the difference between pD and pH (pD = pH + 0.4); in the text all values are reported as pH. After dilution, the protein solutions were centrifuged (3800 g for 8 min). The collected supernatant was filtered with Sartorius filters having a pore diameter of 0.20 μm. The freshly prepared samples in D_2O were divided in several aliquots for FTIR and rheological measurements, in order to characterize the heating phase at 60 °C of native protein solution. D_2O solutions were used to avoid the IR spectral overlaps between Amide I band and the strong water absorption band in the region at around 1650 cm^{-1}.

2.2. FTIR measurements

The first 2 h of BSA incubation were fully characterized through FTIR kinetics at 60 °C. The conformational changes of BSA solutions and the growth of β-aggregates caused by the heating treatment were followed by FTIR measurements continuously or taking small aliquots (30 μL) of the solution samples at different times (15, 30, 60, 120 min, 7 and 20 h). The instrument was a Bruker Vertex 70 spectrometer. The beam splitter is made by KBr and the detector is a DLaTGS (Deuterated L-Alanine Doped Tryglycene Sulphate) with KBr windows. The instrument operated in the mid IR spectral range with a globar light source (i.e. a U-shaped silicon carbide piece) and a spectral resolution of 2 cm^{-1}. Each spectrum was averaged over 100 scans. The errors associated with the determination of the position and amplitude of the IR bands were ±1 cm^{-1} and less than 1%, respectively. The absorption spectrum of the sample-holder (CaF$_2$ windows) and the contribution from buffer absorption were subtracted from the spectrum of each sample. The resultant spectra were smoothed with a 13-point Savitzky-Golay function. The use of D_2O allowed to study the Amide I band and the H/D exchanges between the Amide II and the Amide II′ bands [34]. Deuterated samples were placed between two 2 mm CaF$_2$ windows, with a 0.05 mm teflon spacer.

The conformational changes of the protein secondary structure were obtained by the Amide I composite band. Its profile consists of several spectral components related to the different types of secondary structures [34]. The main band at about 1655 cm^{-1} in the Amide I region is assigned to α-helices. Bands at 1672 and 1681 cm^{-1} reflect the contribution from β–turns, and the band at 1636 cm^{-1} is assigned to β-sheets. Information on the intermolecular aggregation (β-aggregates growth) can be obtained from two shoulders at about 1620 and 1680 cm^{-1} [34] due to the vibrations of the carboxylic groups of β-sheets in intermolecular structures [34]. The information on changes of the tertiary structure was obtained by Amide II and II′ bands (1400-1580 cm^{-1}) [34]. When H-D exchange occurred, an increase of Amide II′ simultaneous to a decrease of Amide II was observed. In order to identify the time evolution of each spectral component under the broad amide bands during infrared kinetics, difference spectra were obtained by subtracting to the spectrum at a generic time t and at a given wavenumber, the spectrum at t_0 (where t_0 was chosen 6 min after the beginning of the experiment to reach the thermal equilibrium) at the same wavenumber:

$$\Delta Abs(t, v) = Abs\,(t, v) - Abs(t_0 - v) \qquad (1)$$

when different aliquots had to be compared, spectra were analyzed using:

$$\Delta Abs(t) = \frac{Abs\left(v_{\beta agg}, t\right)}{Abs(v_{\alpha helix}, t)} - \frac{Abs\left(v_{\beta agg}, t_0\right)}{Abs(v_{\alpha helix}, t_0)} \equiv \Delta\frac{\beta}{\alpha}(t) \qquad (2)$$

where βagg and $\alpha helix$ identify the spectral position of the signal due to the vibrations of intermolecular β-sheets and α-helices structures, respectively.

Structural information on the protein modifications in dependence of pH were monitored by specific infrared bands localized at 1567, 1584, 1706 and 1713 cm^{-1}. These bands are due to the vibration modes of COO$^-$ and C=O of Glutamic (Glu) and Aspartic (Asp) acids, charged residues contributing to the stabilization of the protein structure. Data were made at least in triplicate.

2.3. Rheological measurements

Rheological measurements were performed on a stress controlled AR-G2 rheometer (TA Instruments, USA) using a titanium-cone/plate geometry (angle 0.0174 rad, radius 20 mm, gap 26 μm). Kinetic measurements were obtained from cycles of viscoelastic spectra, with a pause of 50 min, performed in the frequency range 0.02–30 Hz, at a strain of 8×10^{-2}, well within the linear viscoelastic region. The protein suspension at the appropriate pH and at the two concentrations used (0.5 and 1 mM) was gently stirred and placed on the rheometer plate, set at the temperature of 60 °C. The thin sample–air interface was coated with silicone oil to avoid water evaporation. All measurements were done in triplicate both for samples prepared in D$_2$O and H$_2$O to detect effects due to the different solvents.

2.4. Atomic force microscopy

The atomic force microscopy was used to characterize the morphology of the aggregates growing during the incubation leading to the gel formation. Small aliquot (30 μl) of protein solution was deposited on freshly cleaved mica after appropriate dilution. The samples were dried overnight by a gentle nitrogen flux and imaged in air. The instrument used for the AFM measurements in tapping mode was a Veeco MultiMode V Scanning Probe Microscope. Etched-silicon probes with Al-coating on detector side having a pyramidal-shape tip with a nominal curvature <10 nm were used. During scanning, the 125 ± 10 μm long cantilevers, with a nominal spring constant in the range of 40 N/m, oscillated at its resonance frequency (330 kHz). Height, phase and amplitude error images were collected by capturing 512×512 points in each scan,

and the scan rate was maintained below 1 line per second. The worsening of the tips was monitored by using a test pattern before and after every measurement session.

2.5. Scanning Electron Microscopy

The morphology of the final gels was observed by Scanning Electron Microscopy (SEM) with a FEI Quanta 200 FEG Microscope. Gold sputtered samples, previously dehydrated, were observed at 10 KV.

2.6. Cell culture and treatment

Immortalized mouse cerebral endothelial cells, bEnd.3 (American Type Culture Collection, Manassas, VA) were grown in DMEM with 4.5 g/l glucose and supplemented with 10% fetal bovine serum (FBS), 3.7 g/l sodium bicarbonate, and 4 mM glutamine, and 1% antibiotics (penicillin 50 mg/ml and streptomycin 50 mg/ml). LAN5 Neuroblastoma cell line were cultured in RPMI 1640 medium supplemented with 10% FBS and 1% antibiotics (penicillin 50 mg/ml^{-1} and streptomycin 50 mg/ml). Both cellular cultures were maintained in a humidified 37 °C incubator with 5% CO$_2$. The
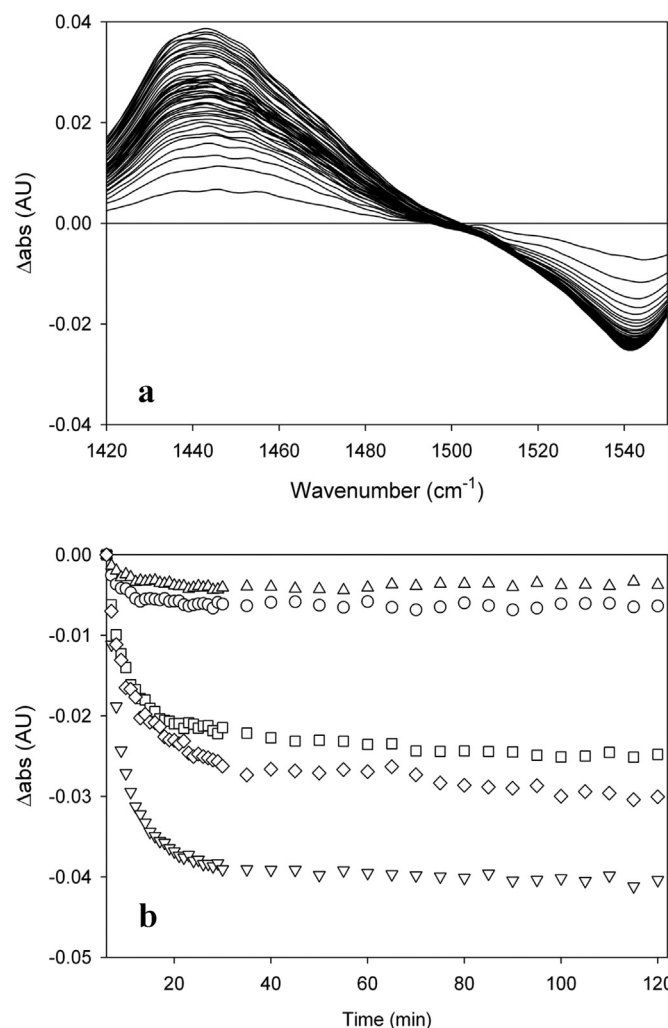
Fig. 2. a) Difference absorption spectra of Amide II and II′ of BSA at 0.5 mM and pH 3.9 incubated at 60 °C. b) Time evolution of the Amide II intensity at 1540 cm^{-1} for BSA solutions at pH 8.5 (triangles up), 7.4 (circles), 5.9 (triangles down), 3.9 (squares) and 2.7 (diamonds).

Fig. 1. Normalized absorption spectra of BSA solution (0.5 mM) prepared at pH 8.5 (dotted line), 7.4 (solid line), 5.9 (dash dotted dotted line), 3.9 (short dashed line) and 2.7 (long dashed line) different pH values. Measurements were made at room temperature.

bEnd.3 cells were pre-seeded at a cell density of 1×10^5 cell/ml in a 96-well plate. After seven days the bEnd3 monolayer was formed and cell-cell junctions were developed. LAN5 cells were pre-seeded on a 96-well plate (1×10^6 cell/ml) and growth for one day. Both cell lines were incubated with the three different synthesized BSA hydrogels capable to supply appropriate mechanical support (pH 3.9, 5.9, 7.4) at two different concentrations (0.5 and 1 mM) for 48 h. After these treatments both the cell lines were submitted to viability assay and microscopic inspection.

2.7. Determination of cell viability

Cell viability was measured by MTS assay (Promega Italia, S. r.l., Milan, Italy). MTS [3-(4,5-dimethylthiazol-2-yl)-5-(3-carboxymethoxyphenyl)-2-(4-sulphophenyl)-2H-tetrazolium], utilized according to the manufacturer's instructions. LAN5 and b. End.3 cells, two models already tested to verify the cell viability after treatment with nanogels systems [35], were treated as described above and after treatment, 20 μL of the MTS solution was added to each well, and the incubation was continued for 1 h at 37 °C in humidified incubator with 5% CO2. The absorbance was read at 490 nm on the Microplate reader Wallac Victor 2 1420 Multilabel Counter (PerkinElmer, Inc. Monza, Italy). Results were expressed as the percentage MTS reduction in the control cells. Moreover, the treated cultured cells and the controls were also morphologically analyzed by microscopic inspection with an Axio Scope2 microscope (ZEISS).

2.8. Statistical analysis

The results shown in cytotoxicity experiments are presented as the mean ± standard deviation (SD). Results were expressed as the percentage MTS reduction in the control cell.

3. Results and discussion

3.1. Characterization of native BSA

The formation of heat-set gel occurs as a consequence of a structural organization of protein aggregates growing during incubation at 60 °C [20,36]. The final characteristics of the gel are highly dependent on the protein conformation [3], pH value [37], as well as on other physical parameters.

In order to monitor the dependence of the protein initial conformation on the pH, FTIR measurements were performed at room temperature for all protein solutions. The protein was diluted in D_2O to allow investigation of the Amide I′ and II′ bands and prepared at different pH values. Absorption spectra performed at 25 °C are reported in Fig. 1.

The data were imaged after normalization at Amide I absorption maximum value. Marked differences in the absorption profile as a function of pH value were revealed at about 1540 cm^{-1}, where the Amide II resulted more intense for BSA at pH 5.9 and 7.4, while it was characterized by a very low intensity at pH far from the isoelectric point of the protein. Moreover, the amplitude of the composite band at about 1575 cm^{-1} markedly decreased at decreasing the pH values. For the samples at acid pH, 3.9 and 2.7, a band at about 1710 cm^{-1} clearly appeared.

These modifications observed as a function of pH change can be interpreted in close connection with the changes of BSA conformational isomerization and charge state [38]. At pH values below 4.3, the BSA conformation was transitioning towards the isomer Fast (F) [38]. It is well known that this isomeric form is characterized by a tertiary structure less compact than the Normal (N) form of BSA, that is the isomeric conformation of the protein when the

pH ranges between 4.3 and 8 [38]. In the transition from N to F isomer, the BSA protein exposes to the solvent the dominium III causing partial opening of the molecule and modification of the protein secondary structure by reduction of the α−helix content, as probed by the slight shift of the Amide I towards lower wavenumbers (Inset of Fig. 1). Because of these structural modifications, at acid pH the internal H atoms of the protein were more easily accessible to the atoms of deuterium (D), thus resulting displaced. This led to an increase of the amide II′ band [1,39] to the detriment of the amide II intensity (Fig. 1). However, at basic pH far from the isoelectric point, due to the increase of the charged residues, the protein assumes a loose tertiary structure.

3.2. Characterization of the structures leading to gelation

FTIR kinetic measurements at 60 °C and at the different pH values and at two protein concentrations have been performed.

In Fig. 2a the difference FTIR spectra of the Amide II and Amide II′ bands as a function of time of the BSA at pH 3.9 are shown. As it is evident, the heating caused the decrease of the Amide II and the
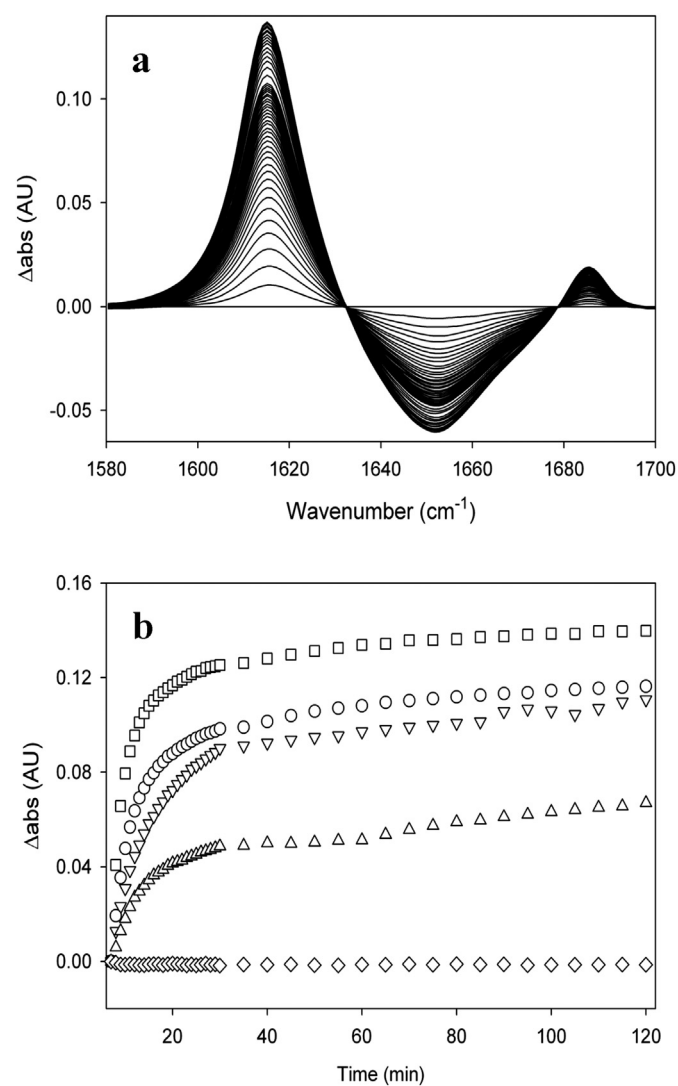
Fig. 3. a) Difference absorption spectra in the spectral range of Amide I of BSA solution 0.5 mM at pH 5.9 incubated at 60 °C. b) Time evolution of absorbance intensity at 1616 cm^{-1} for BSA solutions at pH 8.5 (triangles up), 7.4 (circles), 5.9 (triangles down), 3.9 (squares) and 2.7 (diamonds).
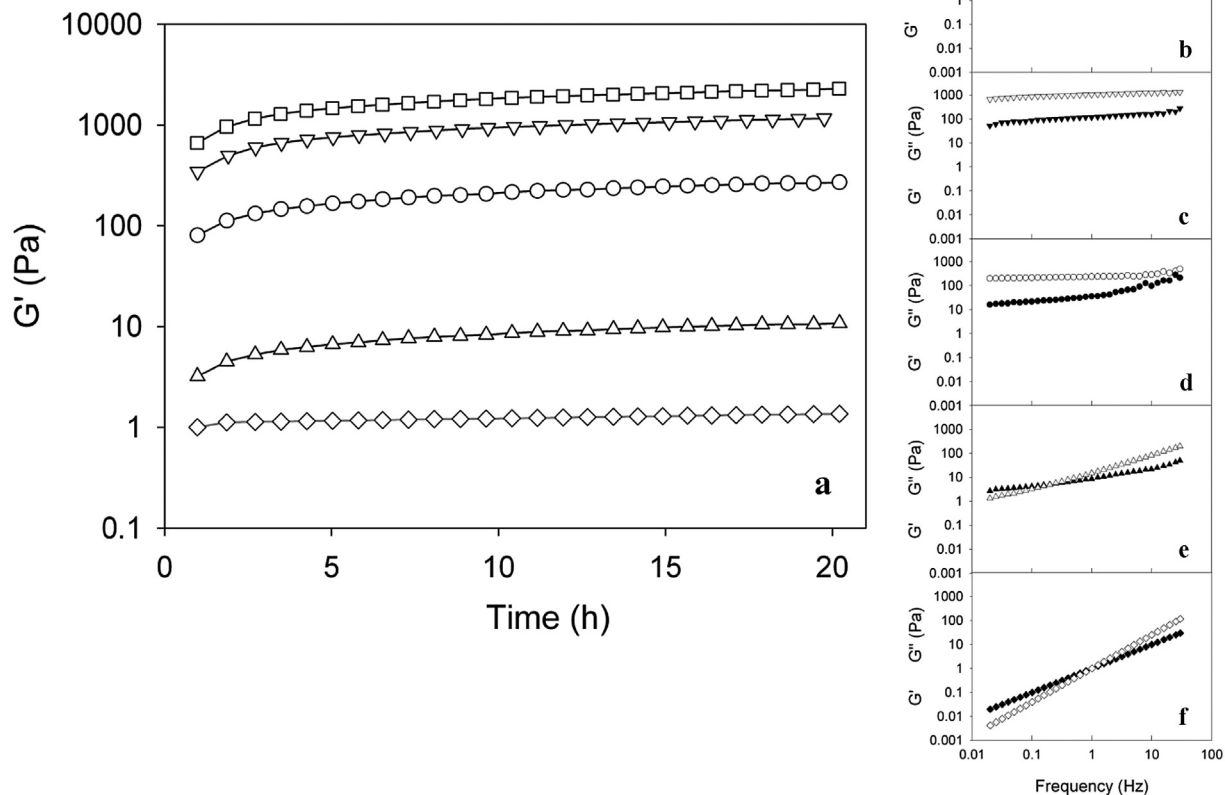
Fig. 4. a) G′ values recorded at 60 °C as a function of time for BSA solutions (1 mM) at pH 3.9 (squares), 5.9 (triangles down), 7.4 (circles), 8.5 (triangles up) and 2.7 (diamonds). G″ values are not reported for an easier reading. The oscillation frequency was 1 Hz and the strain 0.008. b-f) Values of the elastic (empty symbols) and viscous (solid symbols) moduli recorded as a function of the frequency obtained at the end (20 h) of the kinetic measurements for BSA solutions (1 mM) at pH 3.9 (squares), 5.9 (triangles down), 7.4 (circles), 8.5 (triangles up) and 2.7 (diamonds).

simultaneous increase of the Amide II′. The same behavior was common to all samples. The increase of the Amide II′ intensity to the detriment of the Amide II indicated that the heating caused a partial unfolding of the protein molecules. The time evolution of the Amide II intensity at different pH values is reported in Fig. 2b. If for one hand the partial protein unfolding ran out substantially within 40 min at all pH values, on the other hand the extent of the

tertiary structure changes strongly depends on the pH. The observed differences are in agreement with the different native conformations of the protein at different pH [38] as commented in Fig. 1.

The conformational changes of the secondary structure were monitored by the Amide I band.

By the analysis of the difference spectra, reported in Fig. 3a for
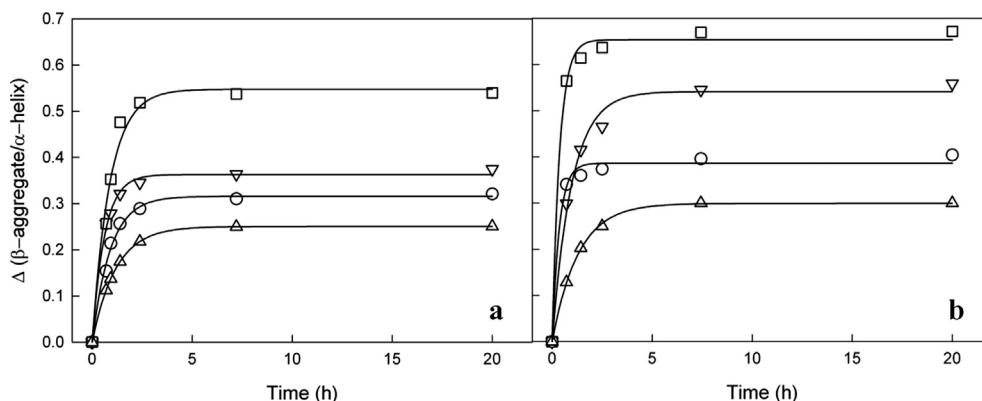
Fig. 5. Time evolution of the relative increase of β-aggregated structures, as obtained by the ratio of the intensities of the bands at 1616 cm^{-1}, related to the β-aggregated structures, and 1655 cm^{-1}, pertinent to α-helices in BSA samples incubated at 60 °C at pH 3.9 (squares), 5.9 (triangles down), 7.4 (circles) and 8.5 (triangles up) at the protein concentrations of 0.5 (a) and 1 mM (b). Solid lines represent the best fit of the experimental points. Data obtained for sample prepared at pH 2.7 are not reported because not significant changes have been recorded during the whole observation time.
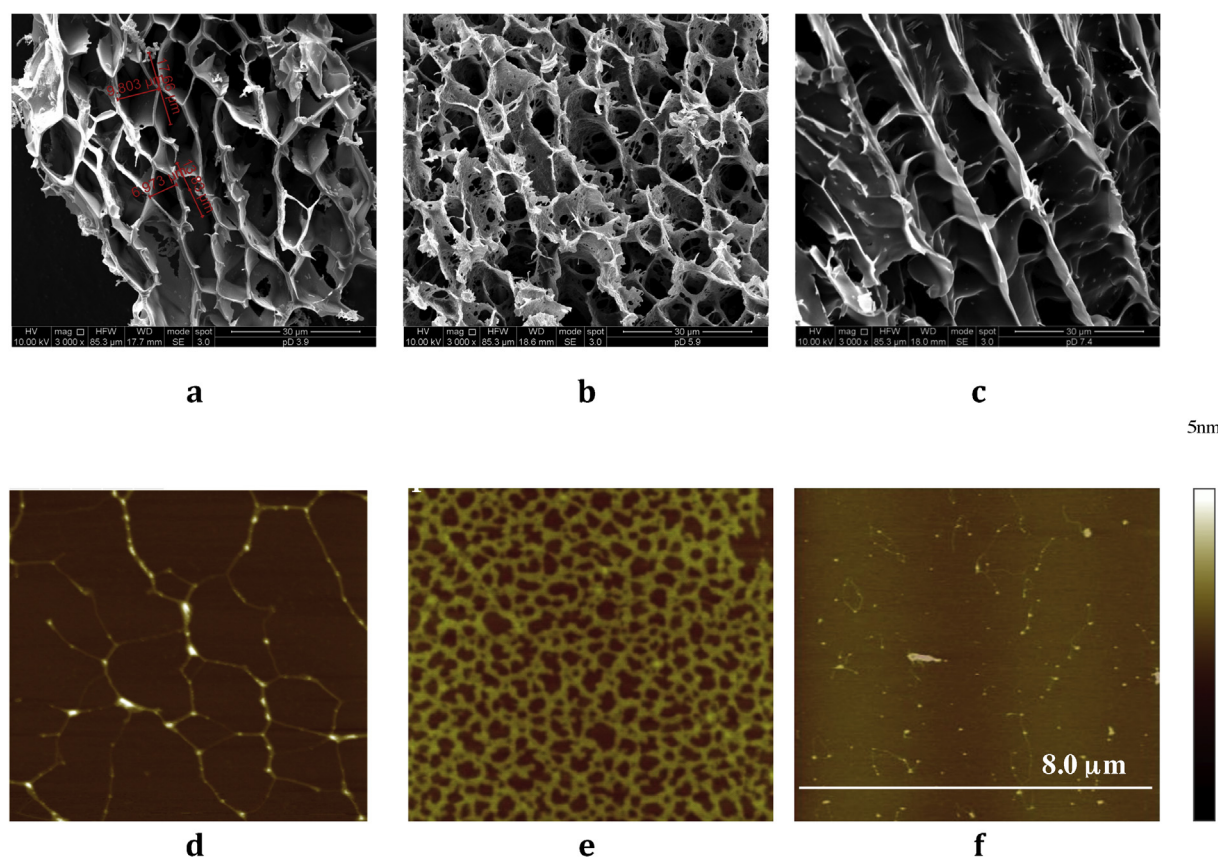
Fig. 6. Morphology of BSA gel prepared at the concentration of 1 mM at pH 3.9 (a, d), 5.9 (b, e) and 7.4 (c, f) after 20 h of incubation at 60 °C as observed by SEM (a–c) and AFM (d–f) experiments. AFM high color scale has maximum at 5 nm. Images were obtained at room temperature.

the BSA at pH 3.9, it can be observed that the heating caused a conversion of α-helix structure band localized at about 1650 cm^{-1} into antiparallel intermolecular β–sheet bands at 1616 and 1685 cm^{-1}. In agreement with our previous results obtained at pH values close to the physiological pH [32,40], no presence of intramolecular β–sheets is observed as indicated by the absence of the band localized at about 1634 cm^{-1}. The same behavior was observed for all samples independently on the pH value, except for BSA at pH 2.7. In this case, the thermal incubation causes a conversion of α-helices in intramolecular β-sheets and no supramolecular aggregate structures could be observed (data not shown). In Fig. 3b, the time evolution of the Amide I intensity at 1616 cm^{-1}, due to the molecular vibrations in the groups involved in the intermolecular β–sheets, is reported. Aggregation was not observed for the BSA sample prepared at pH 2.7, on the contrary a large formation of β-aggregated structures occurred in the BSA solution at pH 3.9. The samples prepared at pH 5.9, 7.4 and 8.5 showed a behavior similar to that observed in the case of pH 3.9, but at a lower extent. Samples prepared at pH 3.9, 5.9, 7.4 and 8.5 exhibited an initial fast growth of the signal and no significant variation of the band intensities were observed after 40 min. For each pH value, similar results were obtained for the samples prepared at the BSA concentration of 1 mM.

3.3. Characterization and morphologies of BSA hydrogels

To investigate about the physical properties of gels prepared at different pH, FTIR, rheological, AFM and SEM measurements were performed on aliquots incubated up to 20 h. The mechanical properties of the BSA samples have been recorded by rheological measurements during 20-h incubation at the different pH values investigated. Rheological results obtained with BSA solutions at the concentration of 1 mM are shown in Fig. 4a–f and discussed. In agreement with FTIR results, the sample prepared at pH 2.7 did not form any macroscopic network up to 20-h incubation at 60 °C as evidenced in Fig. 4a and f. The mechanical spectra, recorded after 20 h exhibited the typical behavior of a viscoelastic liquid with G″ larger than G′, at the lower frequencies and a strong frequency dependence (Fig. 4f). Samples prepared at pH 5.9, 7.4 and especially 3.9 exhibited a marked solid-like character few minutes after the beginning of the kinetic measurements as evidenced by the large initial G′ values (Fig. 4a). Furthermore, mechanical spectra recorded at the end of the incubation time showed the G′ plateau in the whole frequency range explored (Fig. 4b, c and d). A different behavior is exhibited by samples incubated at pH 8.5. In this case, only a weak gel is obtained as indicated by the low G′ values (Fig. 4a). Furthermore, the mechanical spectra displayed that the G′ plateau appears only at frequencies lower than 1 Hz, then the viscous behavior dominated as suggested by the strong frequency dependence and the G″ values greater than those ones of G′ (Fig. 4e). Same results can be obtained at the lower concentration of protein (0.5 mM).

By FTIR spectroscopy, we monitored the growth of the β–aggregated structures to have a deep insight into the gel formation processes. In Fig. 5 the behavior of the ratio of the intensities related to the β–aggregated and α-helices structures as a function of time, for both BSA at 0.5 (Fig. 5a) and 1 mM (Fig. 5b), is reported.

A comparison between both these results suggests that the formation of the macroscopic gel is simultaneous with
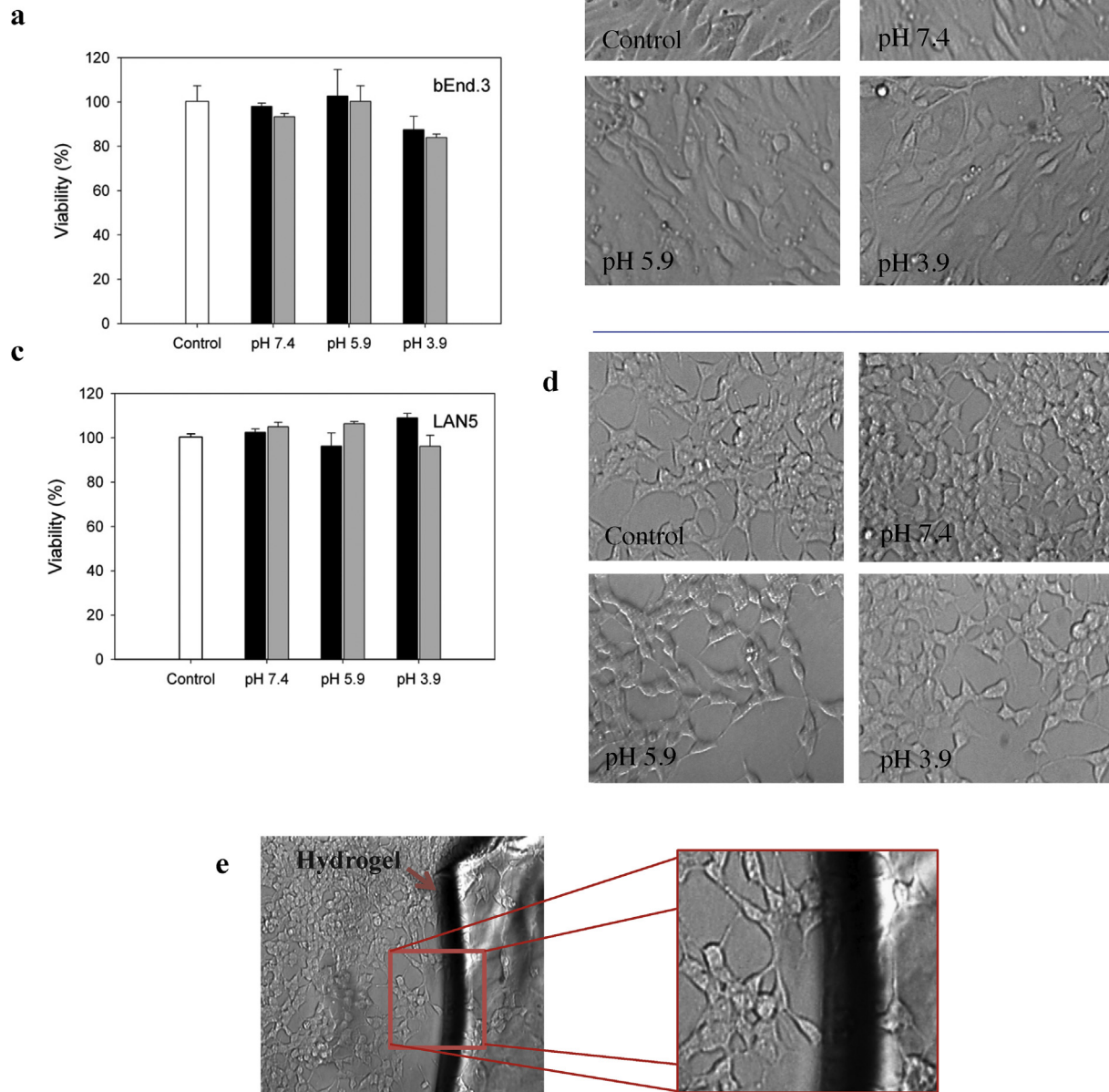
Fig. 7. BSA Hydrogels are cytocompatible. bEnd.3 (a) and LAN5 (c) cell lines incubated with BSA hydrogels at the concentration of 0.5 (black) and 1 mM (gray) and submitted to MTS assay. The results are presented as the mean ± SD. Microscopic inspection of bEnd.3 (b) and LAN5 (d) cells in presence of BSA hydrogels prepared at the concentration of 1 mM at different pH values (7.4, 5.9, 3.9). Representative image of hydrogel deposition on LAN5 neuroblastoma cells.

conformational changes recorded by FTIR measurements within 5 h from the beginning of the protein incubation for all the samples studied.

In order to obtain a characterization of the different 3D network morphologies, SEM and AFM measurements on gel samples with a strong solid-like character have been performed. In Fig. 6a–f images of the sample at pH 3.9, 5.9 and 7.4 are reported.

It could be noted that the gel formed at pH 3.9 (Fig. 6a) presented a well neat structure. Furthermore, the walls of the cages

formed by the network architecture were compact on the contrary of what happened in the case of pH 5.9 where, although the dimensions of the cages were smaller, they seemed sponge-like with the presence several holes. Different aspect had the sample prepared at pH 7.4 in which the microscopic assembly appeared constituted by lamellar structures with few cages. These data were in perfect agreement with results obtained by rheological and FTIR experiments. The gradual lack of compactness was responsible of the different values of the elastic modulus observed in the

rheological experiments and of the lower β-aggregate content recorded at decreasing pH.

AFM images allowed to put in evidence that the BSA hydrogels formed at pH 3.9 and 7.4 were constituted by long and thin fibrillar structures. Moreover, at pH 7.4 numerous oligomers coexisted with long fibrils. Indeed, the BSA hydrogel formed at pH 5.9 was characterized by the presence of thickener fibrils. These different aggregated forms produced a coarser and narrow network in the case of pH 5.9, a well ordered structure for pH 3.9 and a loose structure for pH 7.4.

These morphologies were in agreement with the visual observation of the samples: the gel at pH 5.9 appeared as turbid white, opalescent and firm gels; the gel at pH 3.9 was transparent and strongly firm, evidencing that it was made by a highly ordered structures; the gel at pH 7.4 was transparent too, less firm than that obtained at pH 3.9. In general, the presence of structural order is a plus value to form porous scaffold, a physical support for guiding the formation of new tissue-related extracellular matrix molecules [41].

3.4. Biological properties of BSA hydrogels

The possible use of BSA hydrogels as cell scaffold for tissue engineering applications have been tested on cell model systems. To test in vitro cytotoxicity of BSA hydrogels we utilized endothelial bEnd.3 and neuronal LAN5 cell types. These cells were incubated with two different concentration (0.5 and 1 mM) of the three different BSA synthesized hydrogels, for 48 h. Data reported in Fig. 7a and b, demonstrated that no significant difference in cellular viability was detected for BSA hydrogels in both cell lines at the tested concentrations relatively to the control. The results of the MTS assay were confirmed by microscopic inspection of the untreated and treated cells (Fig. 7c and d). A number of recent studies have revealed that cells sensitively respond to mechanical properties of their environment modifying its adhesion properties (the so-called mechano-response) [42–44]. Fig. 7e is a representative image of the hydrogel deposition on adhered neurobastoma cells. Proximity to or contact of the hydrogel with the cells did not induce any alteration in, neurite outgrowth, extension of cellular body, morphology or contact between cells and cell-substrate. These results suggested that the hydrogels tested are promising candidates for applications in tissue culture.

4. Conclusions

The main aim of the present work has been to determine the best experimental conditions to obtain hydrogels of protein aggregates of BSA at different pH and concentration. In particular, at different pH, we have analyzed the conformational and structural changes of the protein during all the steps of the thermal aggregation and gelation. The mechanical properties of the diverse hydrogels fully agreed with spectroscopic results. Hydrogels morphologies, seen by AFM and SEM techniques, suggested that different arrangement of the protein aggregates lead to different hydrogels network with peculiar properties. The biological tests demonstrated that these gels did not affect the viability of two different cell model systems. Finally, our results indicated that it is possible to modulate the final texture of the hydrogels by tuning the pH value for appropriate tissue engineering applications.

Acknowledgments

References

[1] V. Militello, C. Casarino, A. Emanuele, A. Giostra, F. Pullara, M. Leone, Aggregation kinetics of bovine serum albumin studied by FTIR spectroscopy and light scattering, Biophys. Chem. 107 (2004) 175–187.
[2] H.B. Wijayanti, N. Bansal, H.C. Deeth, Stability of whey proteins during thermal processing: a review, Compr. Rev. Food Sci. Food Saf. 13 (2014) 1235–1251.
[3] X.D. Sun, R.A. Holley, Factors influencing gel formation by miofibrillar proteins in muscle foods, Compr. Rev. Food Sci. Food Saf. 10 (2011) 33–51.
[4] P. Garcia, L. Serrano, M. Rico, M. Bruix, An NMR view of the folding process of a CheY mutant at the residue level, Structure 10 (2002) 1173–1185.
[5] S.W. Englander, Protein folding intermediates and pathways studied by hydrogen exchange, Annu. Rev. Biophys. Biomol. Struct. 29 (2000) 213–238.
[6] L.C. Burnett, B.J. Burnett, B. Li, S.T. Durrance, S. Xu, A lysozyme concentration, pH and time-dependent isothermal transformation diagram reveals fibrous amyloid and non-fibrous, amorphous aggregate species, Open J. Biophys. 4 (2014) 39–50.
[7] D. Saglam, P. Venema, R. de Vries, A. van Aelst, E. van der Linden, Relation between gelation conditions and the physical properties of whey protein particles, Langmuir 28 (2012) 6551–6560.
[8] M. Manno, P.L. San Biagio, M.U. Palma, The role of pH on instability and aggregation of sickle hemoglobin solutions, Proteins Struct. Funct. Bioinforma. 55 (2004) 169–176.
[9] E. Busseron, Y. Ruff, N. Giuseppone, Supramolecular self-assemblies as functional nanomaterials, Nanoscale 5 (2013) 7098–7140.
[10] M. Barbosa, M.C.L. Martins, P. Gomes, Grafting techniques towards productions of peptide-tethered hydrogels, a novel class of materials with biomedical interest, Gels 1 (2015) 194–218.
[11] B. Dhandayuthapani, Y. Yoshida, T. Maekawa, D.S. Kumar, Polymeric scaffolds in tissue engineering applications: a review, Int. J. Polym. Sci. 2011 (2011). Article ID 290602.
[12] S. Kapoor, S.C. Kundu, Silk protein-based hydrogels: promising advanced materials for biomedical applications, Acta Biomater. 31 (2016) 17–32.
[13] I.M. El-Sherbiny, M.H. Yacoub, Hydrogel scaffolds for tissue engineering: progress and challenges, Glob. Cardiol. Sci. Pract. 38 (2013) 317–342.
[14] E. Calò, V.V. Khutoryanskiy, Biomedical applications of hydrogels: a review of patents and commercial products, Eur. Polym. J. 65 (2015) 252–267.
[15] H. Yan, A. Saiani, J.E. Gough, A.F. Miller, Thermoreversible protein hydrogel as cell scaffold, Biomacromolecules 7 (2006) 2776–2782.
[16] S. Gunasekaran, S. Ko, L. Xiao, Use of whey proteins for encapsulation and controlled delivery applications, J. Food Eng. 83 (2007) 31–40.
[17] I. Vhora, S. Patil, P. Bhatt, A. Misra, Protein- and peptide-drug conjugates: an emerging drug delivery technology, in: R. Donev (Ed.), Advances in Protein Chemistry and Structural Biology, Protein and Peptide Nanoparticles for Drug Delivery, vol. 98, Elsevier Academic Press, 2015, p. 3.
[18] C. Du, D. Deng, L. Shan, S. Wan, J. Cao, J. Tian, S. Achilefu, Y. Gu, A pH sensitive doxorubicin prodrug based on folate-conjugated BSA for tumor-targeted drug delivery, Biomaterials 34 (2013) 3087–3097.
[19] Y.-I. Kinekawa, N. Kitabatake, Turbidity and rheological properties of gels and sols prepared by heating process whey protein, Biosci. Biotechnol. Biochem. 59 (1995) 834–840.
[20] J.P. Jung, J.Z. Gasiorowski, J.H. Collier, Fibrillar peptide gels in biotechnology and biomedicine, Biopolymers 94 (2010) 49–59.
[21] D. Hamada, T. Tanaka, G.G. Tartaglia, A. Pawar, M. Vendruscolo, M. Kawamura, A. Tamura, N. Tanaka, C.M. Dobson, Competition between folding, native-state dimerization and amyloid aggregation in β-lactoglobulin, J. Mol. Biol. 386 (2009) 878–890.
[22] J. Juarez, P. Taboada, S. Goy-Lopez, A. Cambon, M.-B. Madec, S.G. Yeates, V. Mosquera, Additional supra-self-assembly of human serum albumin under amyloid-like-forming solution conditions, J. Phys. Chem. B 113 (2009) 12391–12399.
[23] H. Tan, K.G. Marra, Injectable, biodegradable hydrogels for tissue engineering applications, Materials 3 (2010) 1746–1767.
[24] G.M. Shankar, T.H. Metha, A. Garcia-Munoz, N.E. Shepardson, I. Smith, F.M. Brett, M.A. Farrell, M.J. Rowan, C.A. Lemera, C.M. Regan, D.M. Walsh, B.L. Sabatini, D.J. Selkoe, Amyloid-beta protein dimers isolated directly from Alzheimer's brains impair plasticity and memory, Nat. Med. 14 (2008) 837–842.
[25] G.M. Sharkar, A.T. Welzel, J.M. McDonald, D.J. Selkoe, D.M. Walsh, Isolation of low-n amyloid b-protein oligomers from cultured cells, CSF and brain, Methods Mol. Biol. 670 (2011) 33–44.

[26] P. Picone, R. Carrotta, G. Montana, M.R. Nobile, P.L. San Biagio, M. Di Carlo, Abeta oligomers and fibrillar aggregates induce different apoptotic pathways in LAN5 neuroblastoma cell cultures, Biophysical J. 96 (2009) 4200—4211.

[27] V. Vetri, R. Carrotta, P. Picone, M. Di Carlo, V. Militello, Concanavalin A aggregation and toxicity on neuroblastoma LAN5 cell cultures, Biochimica Biophysica Acta Proteins Proteom. 1804 (2010) 173—183.

[28] E.Y. Hayden, D.B. Teplow, Amyloid β-protein oligomers and Alzheimer's disease, Alzheimers Res. Ther. 5 (2013) 60.

[29] I. Benilova, E. Karran, B. De Strooper, The toxic Ab oligomer and Alzheimer's disease: an emperor in need of clothes, Nat. Neurosci. 15 (2012) 349—357.

[30] M.A. Masuelli, Study of Bovine Serum Albumin solubility in aqueous solutions by intrinsic viscosity measurements, Adv. Phys. Chem. 2013 (2013). Article ID 360239.

[31] V. Militello, V. Vetri, M. Leone, Conformational changes involved in the thermal aggregation processes of bovine serum albumin, Biophys. Chem. 105 (2003) 133—141.

[32] G. Navarra, D. Giacomazza, M. Leone, F. Librizzi, V. Militello, P.L. San Biagio, Thermal aggregation and ion-induced cold-gelation of bovine serum albumin, Eur. Biophys. J. 38 (2009) 437—446.

[33] H.J. Shen, H. Shi, K. Ma, M. Xie, L.-L. Tang, S. Shen, B. Li, X.S. Wang, Y. Jin, Polyelectrolyte capsules packaging BSA gels for pH-controlled drug loading and release and their antitumor activity, Acta Biomater. 9 (2013) 6123—6133.

[34] J. Kong, S. Yu, Fourier Transform Infrared Spectroscopic analysis of protein secondary structure, Acta Biochimica Biophysica Sinic. 39 (2007) 549—559.

[35] P. Picone, L.A. Ditta, M.A. Sabatino, V. Militello, P.L. San Biagio, M.L. Di Giacinto, L. Cristaldi, D. Nuzzo, C. Dispenza, D. Giacomazza, M. Di Carlo, Ionizing radiation-engineered nanogels as insulin nanocarriers for the development of a new strategy for the treatment of Alzheimer's Disease, Biomaterials 80 (2016) 179—194.

[36] T. Lefevre, M. Subirade, Molecular differences in the formation and structure of fine-stranded and particulate beta-lactoglobulin gels, Biopolymers 54 (2000) 578—586.

[37] J.P. Celli, B.S. Turner, N.H. Afdhal, R.H. Ewoldt, G.H. McKinley, R. Bansil, S. Erramilli, Rheology of gastric mucin exhibits a pH-dependent sol-gel transition, Biomacromolecules 8 (2007) 1580—1586.

[38] J.F. Foster, Conformational properties of serum albumin, in: V.M. Rosenoer, M. Oratz, M.A. Rothschild (Eds.), Albumin Structure, Function and Uses, Pergamon Press, Oxford (UK), 1977, pp. 53—84.

[39] B.S. Moorthy, L.K. Iyer, E.M. Topp, Characterizing protein structure, dynamics and conformation in lyophilized solids, Curr. Pharm. Des. 21 (2015) 5845—5853.

[40] G. Navarra, A. Tinti, M. Leone, V. Militello, A. Torreggiani, Influence of metal ions on thermal aggregation of Bovine Serum Albumin: aggregation kinetics and structural changes, J. Inorg. Biochem. 103 (2009) 1729—1738.

[41] Z. Qi, Y. Ming, H. Lin, Z. Xin Yuan, L. YunFeng, Y. DeYue, Fabrication of porous scaffolds with protein nanogels, Sci. China Chem. 54 (2011) 961—967.

[42] D.E. Discher, P. Janmey, Y. Wang, Tissue cells feel and respond to the stiffness of their substrate, Science 310 (2005) 1139—1143.

[43] J.A. Engler, S. Sen, H.L. Sweeney, D.E. Discher, Matrix elasticity directs stem cell lineage specification, Cell 126 (2006) 677—689.

[44] S. Even-Ram, V. Artym, K.M. Yamada, Matrix control of stem cell fate, Cell 126 (2006) 645—647.